Published in final edited form as:
Mol Cell. 2013 July 25; 51(2): 141–155. doi:10.1016/j.molcel.2013.06.006.

The telomere deprotection response is functionally distinct from the genomic DNA damage response

Anthony J. Cesare[1], **Makoto T. Hayashi**[1], **Laure Crabbe**[1], and **Jan Karlseder**[1,2]
[1]Salk Institute for Biological Studies, Molecular and Cell Biology Laboratory, 10010 North Torrey Pines Road, La Jolla, California, CA 92037, USA

Summary

Loss of chromosome end protection through telomere erosion is a hallmark of aging and senescence. Here we developed an experimental system that mimics physiological telomere deprotection in human cells and discovered that the telomere deprotection response is functionally distinct from the genomic DNA damage response. We found that unlike genomic breaks, deprotected telomeres that are recognized as DNA damage but remain in the fusion resistant intermediate-state activate differential ATM signaling where CHK2 is not phosphorylated. Also unlike genomic breaks, we found that deprotected telomeres do not contribute to the G2/M checkpoint and are instead passed through cell division to induce p53-dependent G1 arrest in the daughter cells. Telomere deprotection is therefore an epigenetic signal passed between cell generations to ensure that replication-associated telomere-dependent growth arrest occurs in stable diploid G1 phase cells before genome instability can occur.

Introduction

Human telomeres promote genome stability by regulating DNA metabolism at chromosome ends and coopting the DNA damage response (DDR) and DNA repair to limit cellular proliferation in response to telomere erosion (Cesare and Karlseder, 2012). Telomere-dependent controls on cellular proliferation act as a tumor suppressive mechanism by limiting expansion of cell populations harboring precancerous mutations. However, illicit telomere repair can result in chromosome end-to-end fusions that drive genomic instability and oncogenic transformation (Artandi et al., 2000). Telomere-dependent proliferative boundaries therefore rely on carefully balancing DDR activation while limiting chromosomal abnormalities induced by aberrant DNA repair at chromosome ends.

Telomere DNA dynamics are regulated by the “shelterin” protein complex (de Lange, 2010). Conditional deletion of shelterin proteins typically results in acute phenotypes where the chromosome ends are acted upon in a manner similar to genomic breaks. However, the telomeric phenotypes accompanying senescence and crisis are subtler than the acute phenotypes observed in murine knockout models, suggesting that physiological telomere deprotection is mechanistically distinct from telomere dysfunction induced by shelterin deletion.

[2]To whom correspondence should be addressed: karlseder@salk.edu, Phone: (858) 453 4100 ×1867 .

An emerging model suggests spontaneous telomere deprotection during cellular aging progresses through three distinct protective states that regulate cellular consequences (Cesare and Karlseder, 2012). During logarithmic growth “closed-state” telomeres prevent DDR activation by sequestering chromosome termini within a protective higher-order structure, such as a telomere-loop (t-loop) (Griffith et al., 1999). Telomere shortening due to replicative age, or insufficient shelterin saturation, can expose chromosome termini as “intermediate-state” telomeres susceptible to a DDR. However, end joining of intermediate-state telomeres is repressed due to TRF2 retention on the DDR-positive chromatin. Quantitative analysis indicates five or more intermediate-state telomeres in a G1-phase cell is sufficient to induce replicative senescence and more intermediate-state telomeres can accrue in p53 incompetent cells without affecting growth (Kaul et al., 2012). Chromosome fusions occur under physiological conditions at “uncapped-state” telomeres when chromosome ends retain insufficient TRF2 to inhibit end joining. This is expected to occur spontaneously after telomere erosion removes the shelterin binding sites at chromosome ends and is correlated with cell death at crisis.

We recently found that in human cells a specific telomeric DDR also occurs during prolonged mitotic arrest owing to partial dissociation of TRF2 from chromosome ends. This results in an ATM-dependent telomere DDR without chromosome fusions, which activates the prolonged mitotic arrest checkpoint (Hayashi et al., 2012). Following release from the mitotic block p53-competent cells arrest in G1-phase if sufficient numbers of deprotected telomeres are inherited from mitosis.

These observations are consistent with human cells utilizing the transition of closed- to intermediate-state telomeres as a mechanism to arrest proliferation without having to risk the genomic instability associated with chromosome fusions. During cellular aging, such a mechanism likely requires that deprotected telomeres avoid activating the G2/M checkpoint in order to transit cell division and arrest growth in G1-phase. We developed an experimental system to induce intermediate- and uncapped-state telomeres consistent with telomere deprotection observed during cellular aging and found that the telomere deprotection response is functionally distinct from the canonical DDR. Unlike genomic breaks, deprotected telomeres do not contribute to G2/M checkpoint activation and are instead passed through cell division to the G1-phase daughter cells. Also unlike genomic breaks, intermediate-state telomeres induce differential ATM signaling where CHK2 is not phosphorylated. We conclude that telomere deprotection is an epigenetic signal passed between cell divisions that in p53 competent cells functions as a tumor-suppressive and genome-stabilizing mechanism by confining growth arrest to diploid G1 cells. In the absence of p53 transactivation, cells are insensitive to the distinct telomere deprotection signaling, which may promote genome instability and oncogenic transformation.

Results

Experimental induction of intermediate- and uncapped-state telomeres

Observation of physiological telomere deprotection indicates TRF2 has dual functions to safeguard telomeres. It separately prevents ATM activation by sequestering chromosome ends in a closed-state structure and inhibits fusions at intermediate-state telomeres (Cesare et al., 2009). We hypothesized that partial TRF2 depletion below the level required to promote closed-state structure would elicit a telomeric DDR but that retention of some TRF2 would suppress fusions at the DDR(+) intermediate-state telomeres. While complete depletion of TRF2 from chromosome ends would promote fusion of uncapped-state telomeres. To achieve these different outcomes TRF2 was depleted by varying amounts through lentivector transduction of seven different TRF2 shRNAs into IMR90 fibroblasts expressing HPV 16 E6 and E7 (IMR90 E6E7) and HT1080 6TG cells harboring mutant p53 (Figure

1A). Western blots revealed a gradient of TRF2 protein levels following shRNA transduction and the TRF2 shRNAs were designated “sh-A” to “sh-G” in order of increasing knockdown efficiency (Figure 1B and S1A, F). Telomere phenotypes were assessed qualitatively by imaging telomere deprotection induced foci (TIF) in interphase nuclei (Figure 1C) and quantitatively through metaphase-TIF assays (Cesare et al., 2009) and cytogenetic chromosome spreading (Figure 1D and S1A-E). Cultures used for metaphase-TIF assays were treated with 20 ng/ml colcemid for less than one hour, which does not induce TIF (Hayashi et al., 2012; Kaul et al., 2012).

TRF2 sh-A to sh-D resulted in no detectable telomere phenotype (Figure 1D and S1A-E). Metaphase-TIF without concurrent fusions were evident in TRF2 sh-E cultures (Figure 1D and S1A-C). However, TRF2 sh-E also induced separated chromatids with DDR(+) telomeres in IMR90 E6E7 metaphases (Figure S1B), potentially as an off-target effect due to a prolonged mitotic arrest. TRF2 sh-E was thus excluded from further experimentation. TRF2 sh-F induced numerous DDR(+) telomeres with essentially no fusions: i.e. many intermediate-state telomeres (Figure 1D and S1C-E). Whereas TRF2 sh-G induced more DDR(+) telomeres and around ten percent telomere-telomere fusions: i.e. more intermediate-state telomeres than TRF2 sh-F and an appreciable number of uncapped-state telomeres (Figure 1D and S1C-E). Transducing TRF2 sh-F or sh-G into IMR90 E6E7 cells already over-expressing wild-type TRF2 revealed different knockdown efficiencies of the two shRNAs (Figure 1E). Artificially elevating TRF2 levels prior to shRNA transduction also suppressed the associated telomere phenotypes indicating the effects of TRF2 sh-F and TRF2 sh-G were due specifically to reducing TRF2 protein levels below a functional threshold (Figure 1F). ChIP assays confirmed less TRF2 was bound to the telomeres in TRF2 sh-G as compared to TRF2 sh-F cells consistent with the different telomere phenotypes (Figure 1G, H). We have thus generated a system to efficiently induce intermediate-state, or intermediate- and uncapped-state telomeres in human cells dependent upon the efficiency of TRF2 depletion.

Molecular characteristics of intermediate- and uncapped-state telomeres

The DDR at intermediate-state telomeres was ATM-dependent as determined by TRF2 sh expression in AT cells with and without complemented ATM (Figure 1I). H2AX phosphorylation in telomeric chromatin required a chromosome end as γ-H2AX was absent at telomere fusions in mitotic cells (Figure 1J, K). ATM activation at telomeres is consequently the response to exposed chromosome termini serving as activating DDR substrates and not simply a reduction of TRF2 on telomeric chromatin. Because H2AX is dephosphorylated following end joining, interphase-TIF likely represent intermediate-state telomeres, as fused chromosome ends rapidly become γ-H2AX negative. We observed minimal variation in the amount of single-strand G-rich telomeric DNA in TRF2 shRNA transduced cells suggesting telomere overhangs are retained at intermediate-state telomeres and that intermediate-state telomeres are not subjected to extensive end resection (Figure S2A, B).

Four-color imaging confirmed interphase-TIF associate with γ-H2AX and 53BP1 following TRF2 depletion (Figure 1C). The absence of 53BP1 at interphase-TIF following co-depletion of RNF8 or RNF168 indicates ubiquitin signaling promotes 53BP1 recruitment to intermediate-state telomeres (Figure S2C-E) (Jackson and Durocher, 2013). Co-depleting RNF8, RNF168 or Ku80 also reduced the percentage of telomere fusions in TRF2 sh-G cultures in accordance with NHEJ dependent telomere fusions (Figure S2F, G). 53BP1 is thus necessary for fusion of uncapped-state telomeres (Dimitrova et al., 2008) but is also recruited to fusion-resistant intermediate-state telomeres.

Intermediate-state telomeres elicit a differential DDR

Four days post-transduction (Figure 2A and S3A), TRF2 sh-G expression resulted in the concomitant appearance of metaphase-TIF and chromosome fusions (Figure 2B, C and S3B, C), prominent 4C and minor 8C DNA content cell populations (Figure 2D and S3D), and ATM-S1981 and CHK2-T68 phosphorylation (Figure 2E and S3E). A differential response (i.e. a difference in the amount of signaling and phenotypic characteristics) occurred following TRF2 sh-F transduction. The induction of intermediate-state telomeres induced ATM-S1981 phosphorylation, essentially no CHK2-T68 phosphorylation (Figure 2E and S3E) and no change in the cell cycle profile (Figure 2D and S3D). Despite numerous deprotected telomeres, cells in TRF2 sh-F and sh-G cultures continued to enter mitosis as indicated by H3-S10 phosphorylation (Figure 2E and S3E), whereas the parental cells effectively activated the G2/M checkpoint in response to irradiation (IR) (Figure 2E and S3E).

The concurrent appearance of telomere-fusions and accumulated cells with 4C and 8C DNA content in the absence of G2/M checkpoint activation suggests some 4C cells in TRF2 sh-G cultures are tetraploid G1-phase cells that have undergone genome duplication. We confirmed this by identifying via flow cytometry an increase in Cyclin B1 negative 4C DNA content cells and cycling cells with ≥ 4C DNA content in TRF2 sh-G cultures (data not shown). Internuclear chromatin bridges and binucleation were common in TRF2 sh-G cultures (see below and data not shown) suggesting genome duplication stemmed from cytokinesis failure due to telomere fusions resulting in chromatin in the cleavage furrow (Pampalona et al., 2012). Diplo-chromosomes were not observed in any TRF2 sh cultures (data not shown). The absence of prominent 4C and 8C peaks in the TRF2 sh-F cultures indicates that an ATM-dependent telomere DDR does not promote genome duplications in the absence of telomere fusions.

TRF2 depletion does not affect the G2/M checkpoint

To ensure TRF2 depletion does not affect G2/M checkpoint activation we treated control and TRF2 sh expressing cells with low dose IR and assayed for growth arrest. Consistent with the canonical DDR, a reduction of H3-S10 phosphorylation was evident following IR treatment of HT1080 6TG TRF2 sh-F and sh-G, as well as IMR90 E6E7 TRF2 sh-F cells (Figure 2F and S3F). IR treatment of TRF2 sh-F cultures also induced CHK2-T68 phosphorylation, indicating the differential DDR from intermediate-state telomeres was not due to TRF2 sh-F effecting CHK2 function (Figure 2F and S3F). IR treatment also increased the percentage of 2C and 4C content cells in control and TRF2 sh-F cultures, consistent with both G1/S and G2/M checkpoint activation (Figure 2G and S3G). In TRF2 sh-G cultures the percentage of cells in the 2C, 4C and 8C peaks increased following IR treatment, in agreement with G1/S and G2/M arrest in cells with the normal and duplicated chromosome complement (Figure 2G and S3G). Flow cytometry measurement of H3-S10 phosphorylation positive cells indicated that HT1080 6TG TRF2 sh-F and sh-G and IMR90 E6E7 sh-F cells all exhibited similar activation of, and recovery from, the G2/M checkpoint following IR treatment (Figure 2H and S3H). We note that as fusions accumulated in IMR90 E6E7 TRF2 sh-G cultures, mitotic duration extended, resulting in an increase of mitotic cells in the population (Figure S3H and data not shown).

53BP1-S25 was phosphorylated in TRF2 sh-F and TRF2 sh-G cultures in response to telomere deprotection (Figure 2F and S3F) consistent with ATM-dependent N-terminal 53BP1 phosphorylation functioning to recruit RIF1 and preventing end-resection at intermediate-state telomeres (Chapman et al., 2013; Escribano-Diaz et al., 2013). Similar to CHK2, NBS1-S343 was not phosphorylated in TRF2 sh-F cultures without IR treatment

(Figure 2F and S3F) consistent with NBS1 phosphorylation contributing to the intra-S checkpoint that is not activated by the differential DDR (Lim et al., 2000).

Deprotected telomeres are passed through cell division

The absence of telomere-deprotection dependent G2/M checkpoint activation suggests deprotected telomeres pass through cell division. We checked this by synchronizing cultures in G1/S, releasing, and collecting samples for analysis every two hours until the cultures re-entered G1 (Figure 3A and S4A). Following release, IMR90 E6E7 control sh and TRF2 sh-F cultures exhibited similar kinetics of cell cycle progression (Figure 3A). Diploid IMR90 E6E7 TRF2 sh-G cells also progressed through the cell cycle with similar kinetics. Though a prominent 4C peak was present at all times in the IMR90 E6E7 sh-G cultures consistent with tetraploid G1-phase cells that failed to initiate DNA replication (Figure 3A). All HT1080 6TG cultures contained some 4C G1 phase cells after synchronization, as confirmed by the progression of 4C peaks to 8C during S and G2, then back to 4C following cell division (Figure S4A). Telomere-fusions exaggerated the number of 4C G1 phase cells in HT1080 6TG TRF2 sh-G cultures. All HT1080 6TG cultures progressed through cell division with similar kinetics with only a minor delay in mitotic entry in TRF2 sh-G being observed by nuclear imaging (Figure S4A).

G1/S synchronized cultures exhibited pan nuclear or speckled γ-H2AX and 53BP1 staining indicative of stalled replication forks (Figure 3A and S4A). In addition, synchronized TRF2 sh-F and sh-G cultures also had a distinct cell population with prominent DDR foci typically containing multiple telomeres. We anticipate these nuclei, which were only present in the TRF2 sh-F and sh-G cultures, represent G1 arrested cells that failed to replicate after synchronization. Following release from synchronization the speckled γ-H2AX and 53BP1 foci in control sh cultures rapidly disappeared as cells progressed through the cell cycle. In contrast, following release in TRF2 sh-F and TRF2 sh-G cultures, γ-H2AX and 53BP1 quickly became localized in punctate foci at telomeres as the cells progressed through S and G2. Unlike the TIF in most nuclei in asynchronous cultures or the prominent TIF in the G1-arrested cells during synchronization where large DDR foci contain multiple telomeres, TIF in synchronized S- and G2-phase cells were small and contained individual telomeres. 53BP1 dissociated from γ-H2AX(+) telomeres at the G2/M boundary and was present as a diffuse cytoplasmic signal while the γ-H2AX associated telomeres were segregated to the daughter cells during cell division (Figure 3B). Telomeres associated with the nuclear periphery in G1 following cell division (Crabbe et al., 2012) and 53BP1 re-associated with the γ-H2AX(+) telomeres in prominent TIF often containing multiple telomeres.

We confirmed cells with deprotected telomeres entered mitosis and segregated their deprotected telomeres during cell division through live-cell imaging of HeLa 1.2.11 cells expressing GFP-TRF1 and mCherry-BP1-2, a fragment of 53BP1 that localizes to deprotected telomeres (Dimitrova et al., 2008). Time-lapse imaging of asynchronous TRF2 sh cultures revealed numerous cells where mCherry-BP1-2 associated telomeres were evident prior to mitosis, the mCherry-BP1-2 protein dissociated from the telomeres at the mitotic boundary and then re-associated with telomeres after cell division (Figure S4B and Movie S1-4).

The G2/M checkpoint is more relaxed than the G1/S checkpoint, allowing cells with up to 20 γ-H2AX foci to enter mitosis (Deckbar et al., 2007). The passage of deprotected telomeres from G2 into mitosis suggests the number of metaphase-TIF in asynchronous cultures represents the number of deprotected telomeres inherited from the previous G2. We found that mitotic TRF2 sh-F and sh-G cells commonly contained many more than 20 γ-H2AX labeled telomeres indicating the passage of deprotected telomeres into mitosis was not simply due to a relaxed G2/M checkpoint (Figure 3C). Moreover, TRF2 sh-F or sh-G did

not sensitize cells to IR-induced G2/M arrest (Figure 3D), indicating that unlike genomic breaks the ATM-dependent telomere DDR does not contribute to G2/M checkpoint activation.

Differential telomere DDR signaling induces p53-dependent G1-phase arrest

We addressed how telomere deprotection arrests cell growth in p53 competent cells by transducing primary IMR90 fibroblasts with control sh, TRF2 sh-F or TRF2 sh-G (Figure 4A). TRF2 sh-F induced only a modest TIF phenotype in IMR90 cells (Figure 4B, C) with no detectable p53 accumulation (Figure 4D) and a limited reduction of cell proliferation (Figure 4E). TRF2 sh-G, however, induced a robust TIF phenotype (Figure 4B, C), p53 and p21 accumulation (Figure 4D), a major reduction in cell proliferation (Figure 4E) and the accumulation of G1-phase cells (Figure 4F) with a senescent morphology (data not shown). While TRF2 sh-G induced intermediate- and uncapped-state telomeres in p53 incompetent cells, several lines of evidence suggest TRF2 sh-G was less effective in IMR90 cells and induced growth arrest via intermediate-state telomeres. First, TRF2 sh-G induced ATM-S1981 phosphorylation without CHK2-T68 phosphorylation in IMR90 cells consistent with the differential DDR from intermediate-state telomeres (Figure 4D). Persistent interphase TIF seven days post-transduction in IMR90 TRF2 sh-G cultures are also consistent with intermediate-state telomeres (Figure 4B, C) because H2AX is dephosphorylated in telomeric chromatin following end joining (Figure 1F, G). Minimal inter-nuclear chromatin bridges in IMR90 TRF2 sh-G cultures further support little telomere fusion in these cells (Figure 4G, H). We were unable to determine why TRF2 sh-F was not more effective in IMR90 cultures.

Despite the absence of CHK2-T68 phosphorylation, TRF2 sh-G induced p53 and p21 accumulation (Figure 4D) indicating the differential DDR from intermediate-state telomeres is sufficient to restrict cell proliferation in p53 competent cells. To confirm differential DDR signaling from intermediate-state telomeres was not simply the result of reduced input into the DDR pathway, we treated parental IMR90 cultures with a gradient of low dose IR. In these experiments ATM-S1981, CHK2-T68 and p53-S15 phosphorylation accumulated with similar kinetics (Figure 4I), indicating that genomic breaks induce the canonical DDR signaling pathway even with a very low dose of damage. This again emphasizes that intermediate-state telomeres result in a differential response that is not functionally equivalent to induced genomic breaks.

Intermediate-state telomeres passed through mitosis arrest growth in G1

The lack of telomere deprotection induced G2/M arrest suggests G1 arrest in IMR90 TRF2 sh-G cultures is due in part to G1-phase cells inheriting deprotected telomeres from the preceding cell cycle. We tested this by transducing IMR90 cells with control sh or TRF2 sh-G and collecting samples from days three to seven post-transduction (Figure 5A). TRF2 sh-G induced concomitant accumulation of ATM-S1981 and p53-S15 phosphorylation, p53 and p21 protein levels, and the reduction of H3-S10 phosphorylation in the absence of CHK2-T68 phosphorylation in agreement with the differential DDR from intermediate-state telomeres (Figure 5B). Consistent with G1-phase arrest we observed an increase in 2C DNA content cells and a reduction of S-phase cells coincident with DDR activation in IMR90 TRF2 sh-G cultures four days post-transduction (Figure 5C, D). Examination of mitotic cells in IMR90 TRF2 sh-G cultures at 3.5 days post-transduction, corresponding to the onset of G1 arrest, revealed numerous DDR(+) telomeres (Figure 5E, F). Quantitation of metaphase-TIF indicated 56 ± 11% of TRF2 sh-G metaphases had ≥ 10 γ-H2AX associated telomere chromatids (Figure 5F), which following random segregation would be expected to transfer five or more deprotected telomeres to the G1-phase daughter cells and arrest growth (Kaul et al., 2012). In addition, 20 ± 12% of metaphases had ≥ 20 γ-H2AX associated telomeres, consistent with no telomere-dependent G2/M checkpoint activation.

A recent report suggested that TRF2 siRNA transfection in p53 competent cancer cells induced a p53-dependent G2/M arrest through cdc25c degradation (Thanasoula et al., 2012). We also observed a reduction in cdc25c protein levels following TRF2 depletion but note that this happens in G1-phase arrested cultures (Figure 5A-C), indicating cdc25c degradation occurs through a mechanism unrelated to the G2/M checkpoint. An alternative explanation is that the reduction of mitotic cells and p53 activation following TRF2 siRNA treatment was due to G1-phase arrest and cells not entering the cell cycle as observed here.

Prolonged mitotic arrest induces intermediate-state telomeres

To test the effects of prolonged mitotic arrest on telomeres (Hayashi et al., 2012) we synchronize cells with a double thymidine block, release and dose the cultures with 100 ng/ml colcemid at six hours after release when the cells are in S/G2. Synchronized cultures enter mitosis between 8 and 10 hours after release. When mitotic cells are collected 10 hours after release, corresponding to ≤ two hours of mitotic arrest, there is no difference in metaphase-TIF in colcemid(+) and colcemid(−) samples. In contrast, mitotic cells collected 16 hours after release, corresponding with six to eight hours of mitotic arrest, exhibit a pronounced increase in metaphase-TIF (Hayashi et al., 2012). We sought to determine if telomere deprotection during prolonged mitotic arrest induced a canonical or differential DDR.

Examination of IMR90 cells revealed that some TRF2 was retained at the γ-H2AX(+) telomeres during prolonged mitotic arrest (Figure 6A, B) similar to intermediate-state telomeres in aged primary cells (Kaul et al., 2012). Consistent with a differential DDR, ATM-S1981 phosphorylation accumulated in cells during a prolonged mitotic arrest without accumulation of CHK2-T68 phosphoyrlation either during the mitotic block or after release and entry into G1 (Figure 6C). Prolonged mitotic arrest induces a partial TRF2 dissociation from the telomeric chromatin. Consistent with this, TRF2 sh-F cultures depleted of TRF2 exhibited a more pronounced increase in metaphase-TIF than control shRNA cultures subjected to the same mitotic duration (Figure 6D, E and S5).

Treating cultures with Hesperadin before an extended mitosis suppresses Aurora B activity and metaphase-TIF accumulation, demonstrating telomere deprotection during prolonged mitotic arrest is Aurora B dependent (Hayashi et al., 2012). We predicted that Hesperadin treatment should allow us to discriminate between metaphase-TIF that accrue during mitotic arrest and TIF carried into mitosis from the preceding G2. As predicted, Hesperadin treatment suppressed TIF accumulation during prolonged mitosis in control and TRF2 sh-F cultures, but not the passage of intermediate-state telomeres from G2-phase into mitosis (Figure 6E and S5).

Despite the elevated numbers of metaphase-TIF in IMR90 E6E7 TRF2 sh-F cells following prolonged mitosis we did not observe an increase in fusions when mitotically arrested cells were collected by shake-off, replated and cultured for 36 hours (Figure 6F). Consistent with a differential DDR in the absence of fusions, TRF2 sh-F cultures exhibited ATM-S1981 phosphorylation with only a minor accumulation of CHK2-T68 phosphorylation following prolonged mitotic arrest, release and entry into G1 (Figure 6G). These data indicate that the amount of telomere bound TRF2 is critical to suppress the conversion of closed-state to intermediated-state telomeres, while the conversion from intermediate-state to uncapped-state telomeres is very rare even with exceedingly limited amounts of TRF2.

DDR signaling at senescence is consistent with intermediate-state telomeres

Previous observations indicated five intermediate-state telomeres correlate with senescence induction in human cells (Kaul et al., 2012). To determine if senescence is induced by the

differential DDR from intermediate-state telomeres we cultured primary IMR90 and WI-38 fibroblasts in hypoxic conditions and prepared whole cell extracts from untreated and irradiated cultures at different population doublings until replicative senescence (Figure 7A). As cultures aged they displayed increased p53 and p21 accumulation, reduced H3-S10 phosphorylation, and reduced Histone H3 and H4 production, consistent with an increasing percentage of senescent cells in the population (O'Sullivan et al., 2010) (Figure 7B,C). In agreement with a differential DDR, aging cells exhibited no spontaneous CHK2-T68 phosphorylation in non-irradiated cultures approaching senescence (Figure 7B, C). Minor amounts of CHK2-T68 phosphorylation were only observed in unirradiated primary cultures after senescent IMR90 cells were maintained in the same culture dish for 14 days well after proliferation had ceased (Figure 7B).

Subjecting aged IMR90 cultures to prolonged mitotic arrest increased the number of metaphase-TIF (Figure 7D and S6). By treating the aged cells with Hesperadin prior to the mitotic block we suppressed TIF accumulation during mitosis, revealing the elevated number of spontaneous metaphase-TIF that are passed into mitosis from the previous G2-phase in aged IMR90 cells (Figure 7D). These results are consistent with previous observations of spontaneous telomere deprotection in aged cells (Kaul et al., 2012) and indicate that these deprotected mitotic telomeres were inherited from the previous G2-phase. The lack of telomere-dependent G2/M arrest in aged cells was further demonstrated by comparing cell cycle progression of young and old IMR90 cells following synchronization and release from a double thymidine block. While more cells in the aged cultures failed to enter S-phase after synchronization, those that did progressed through the cell cycle with similar kinetics as the young culture indicative of no telomere-dependent G2/M arrest (Figure 7E). Lastly, when IMR90 E6E7 cells were passaged until crisis, we only observed spontaneous CHK2-T68 phosphorylation in non-irradiated cultures during the lifespan extension phase of growth, consistent with the spontaneous occurrence of uncapped-state telomeres (Figure 7F).

Discussion

In this study we discovered that intermediate-state telomeres induce a differential DDR where CHK2 is not phosphorylated in human fibroblasts and a fibrosarcoma cell line. Unlike genomic breaks, deprotected telomeres do not contribute to the G2/M checkpoint but are instead passed through cell division, suggesting that intermediate-state telomeres are an epigenetic response passed across cellular generations to ensure telomere-dependent growth arrest is confined to diploid G1-phase cells.

TRF2 has multiple protective functions at human telomeres

Our data are consistent with TRF2 exerting separate protective functions to suppress ATM activation by hiding chromosome termini within closed-state structures and to inhibit fusion of DDR(+) telomeres. TRF2 thus modulates the accessibility of chromosome termini as ATM activating substrates but does not inhibit ATM from phosphorylating H2AX once it is active at the telomeric chromatin. The DDR response at intermediate-state telomeres is therefore an epigenetic response to telomere structural changes which has previously been implicated as the activator of replicative senescence (Karlseder et al., 2002).

A mechanism for the separation of TRF2 protective functions was recently suggested to result from a small motif in TRF2 suppressing chromatin ubiquitination by RNF168 to prevent 53BP1 localization (Okamoto et al., 2013). We always observe γ-H2AX and 53BP1 localization to intermediate-state telomeres in interphase nuclei. However, this apparent discrepancy can be reconciled. The small difference in TRF2 protein abundance between TRF2 sh-F and TRF2 sh-G cells suggests very little TRF2 protein is required to prevent end

joining. The sensitivity of TRF2 protection against fusion could be explained by TRF2 being retained specifically at the distal telomere end, supported by experiments suggesting TRF2 has binding preference to the single-strand/double-strand junction (Stansel et al., 2001). Preferential binding of TRF2 to the distal chromosome end would also ensure the greatest protection against fusions. At intermediate-state telomeres, distal TRF2 likely limits RNF168 dependent ubiquitination at the terminal telomere nucleosomes. Ubiquitination of proximal telomeric or sub-telomeric chromatin not bound by TRF2 would result in 53BP1 recruitment visualized here as co-localization with γ-H2AX. 53BP1 recruitment to intermediate-state telomeres may also be critical to recruit RIF1 and prevent extensive resection of the telomeric DNA. As additional TRF2 protein nucleates proximally from the chromosome end we anticipate this will establish the closed-state structure.

Differential versus canonical DDR signaling from deprotected telomeres

Deprotection via the intermediate-state confers a specialized chromatin environment where checkpoint signaling is limited. Our discovery of a differential DDR allows speculation that TRF2 directly interacts with ATM and/or CHK2 to limit CHK2 phosphorylation, consistent with reports detailing interactions between TRF2 and these kinases (Buscemi et al., 2009; Karlseder et al., 2004). A second possibility is that full activation of ATM signaling requires chromatin modifications inhibited by TRF2 at intermediate-state telomeres. This is supported by reports detailing how ablation of ubiquitin signaling associated with DSB repair suppresses ATM activity (Wu et al., 2011), that ATM localization to telomeres stripped of TRF2 is tempered in RNF8 depleted cells (Peuscher and Jacobs, 2011) and that TRF2 inhibits chromatin ubiquitination (Okamoto et al., 2013). Also possible is that human telomeres are a privileged environment lacking constitutive chromatin modifications necessary to elicit a full DDR (Carneiro et al., 2010).

Once low TRF2 levels render the telomere in the uncapped-state, the fusion sensitive telomere is capable of activating CHK2 phosphorylation, as has been shown by murine models in cells void of TRF2 (Celli and de Lange, 2005; Celli et al., 2006). We expect the canonical DDR signaling observed in TRF2 sh-G cultures and during life-span extension results from uncapped-state telomeres and telomere-fusion dependent genomic instability.

Intermediate-state telomeres likely avoid G2/M arrest by limiting CHK2 activation. How cells with uncapped-state telomeres avoid G2/M arrest is not as clear, but cell cycle dependent control over DNA break repair likely holds the answer. In G2, when recombination is most active, the POT1/TPP1 heterodimer likely limits resection at deprotected chromosome ends to prevent ATR activation (Denchi and de Lange, 2007; Gong and de Lange, 2010).

Intermediate-state telomeres are tumor suppressive and genome protective

Progressive telomere erosion during replicative aging dictates that telomeres deprotect through the intermediate-state before reaching the uncapped-state, therefore constraining senescence to diploid G1-phase cells. This prevents genome instability by inducing arrest before genomes become destabilized through telomere fusions. Deprotection through the intermediate-state and G2/M checkpoint avoidance are thus critical normal functions of human telomeres to ensure healthy genomes as cells age. This comes with the price of p53 activation by intermediate-state telomeres, contributing to tissue degradation in the telomere syndromes and during the aging program (Armanios and Blackburn, 2012; Lee et al., 1998).

It has been known for sometime that losing p53 cooperates with telomere dysfunction to drive oncogenesis, though the underlying mechanism remained unclear (Chin et al., 1999). We have now solved this problem. As demonstrated here, telomere deprotection does not

activate a G2/M block in human cells. Therefore, once p53 transactivation is lost and the cells become insensitive to G1/S arrest (Deng et al., 1995; Waldman et al., 1995), there remains no mechanism to halt the cell cycle in response to telomere deprotection. Cells in the lifespan extension phase of growth, or cancer cells that lack p53 activity, can proliferate with impunity despite numerous intermediate-state telomeres (Cesare et al., 2009; Kaul et al., 2012). Continued telomere erosion during lifespan extension will eventually result in end-to-end fusions. However, cell death during life-span extension relies on a precarious mechanism where lethality is dependent on telomere-fusion driven genomic instability. If genomic changes during this period upregulate a telomere length maintenance mechanism before cell death occurs, this will provide sufficient TRF2 binding sites at chromosome ends to rescue the cell from crisis and confer immortality.

Experimental Procedures

Cell Culture and treatments

We obtained IMR90 cells from ATCC, AT22IJET cells from Matt Weitzman (University of Pennsylvania), and HT1080 6TG cells from Eric Stanbridge (UC-Irvine). Cells were cultured as described (O'Sullivan et al., 2010). 1μg/ml puromycin (Corning Cellgro) was used to select for lentivector transduction. Cell synchronization and treatments were performed as described (Hayashi et al., 2012).

Vectors

TRF2 shRNAs in pLKO.1 vectors were obtained from Open Biosystems and correspond to the following clones: TRF2 sh-A (TRCN0000004810), sh-B (TRCN0000004813), sh-C (TRCN0000004812), sh-D (TRCN0000018360), sh-E (TRCN0000004809), sh-F (TRCN0000004811) and sh-G (TRCN0000018358). The non-coding control shRNA was obtained from David Sabatini via Addgene (plasmid 1864).

Flow cytometry

Samples were prepared and the data collected as described (Hayashi et al., 2012).

Fluorescent imaging and analysis

Imaging techniques were performed as described (Cesare et al., 2009). Four-color imaging was performed using a Zeiss Axioimager Z1 with an apoptome. Displayed images of adherent cells are maximum intensity projections of two to four Z-planes for interphase nuclei and six to ten Z-planes for mitotic cells, with each plane separated by 0.3 ≥m. For metaphase analysis, ≥ 25 metaphases were quantified for each metaphase-TIF experimental replicate and ≥ 30 metaphases for each cytogenetic preparation experimental replicate.

Western blots and ChIP

Western blots and ChIP assays performed as described (O'Sullivan et al., 2010).

Antibodies

Actin (Sigma AC15); ATM (Epitomics 1549-1); ATM-S1981 (Epitomics EP1890Y and Rockland 200-301-400); cdc25c (Santa Cruz sc-327); CHK2 (Millipore 05-649); CHK2-T68 (Cell Signaling Technology 2661); H3 (Abcam ab1791); H3-S10 (Cell Signaling Technology 3377); H3-S10 Alexa Flour 488 conjugated (Cell Signaling Technology 3465); H4 (Abcam ab7311); H2AX (Abcam ab11175); γ-H2AX (Millipore 05-636, Bethyl A300-081A and Biolegend, 613402); NBS1 (GeneTex GTX70222); NBS1-S343 (Cell Signaling Technology 3001); p21 (Millipore 05-655); p53 (Santa Cruz sc-126); p53-S15 (Cell Signaling Technology 9284); TRF2 (Karlseder lab); 53BP1 (Santa Cruz sc-22760) and

53BP1-S25 (Bethyl A300-652A). We used highly cross-absorbed secondary antibodies conjugated to Alexa Flour 488, Alexa Flour 564 or Alexa Flour 647 (Life Technologies) and secondary antibodies conjugated to HRP (GE healthcare).

Supplementary Material

Refer to Web version on PubMed Central for supplementary material.

Acknowledgments

We thank the Salk Institute's James Fitzpatrick of the Waitt Advanced Biophotonics Center, Daniel Gibbs of the GT3 core, and David Chambers of CCMI for their expertise. A.J.C. is supported by an NIH NRSA T32 Fellowship (5T32CA009370-29), M.T.H. by fellowships from the Human Frontier Science Program and the Japan Society for the Promotion of Science Postdoctoral Fellowships for Research Abroad, and L.C. by a fellowship from the Salk Institute Glenn Center for Aging. The Karlseder laboratory is supported by the Salk Institute Cancer Center Core Grant (P30 CA014195-38), the NIH (GM087476), the John Sabo Trust and the Highland Street Foundation.

References

Armanios M, Blackburn EH. The telomere syndromes. Nature reviews. Genetics. 2012; 13:693–704. [PubMed: 22965356]

Artandi SE, Chang S, Lee SL, Alson S, Gottlieb GJ, Chin L, DePinho RA. Telomere dysfunction promotes non-reciprocal translocations and epithelial cancers in mice. Nature. 2000; 406:641–645. [PubMed: 10949306]

Buscemi G, Zannini L, Fontanella E, Lecis D, Lisanti S, Delia D. The shelterin protein TRF2 inhibits Chk2 activity at telomeres in the absence of DNA damage. Curr Biol. 2009; 19:874–879. [PubMed: 19375317]

Carneiro T, Khair L, Reis CC, Borges V, Moser BA, Nakamura TM, Ferreira MG. Telomeres avoid end detection by severing the checkpoint signal transduction pathway. Nature. 2010; 467:228–232. [PubMed: 20829797]

Celli GB, de Lange T. DNA processing is not required for ATM-mediated telomere damage response after TRF2 deletion. Nature cell biology. 2005; 7:712–718.

Celli GB, Denchi EL, de Lange T. Ku70 stimulates fusion of dysfunctional telomeres yet protects chromosome ends from homologous recombination. Nature cell biology. 2006; 8:855–890.

Cesare AJ, Karlseder J. A three-state model of telomere control over human proliferative boundaries. Current opinion in cell biology. 2012; 24:731–738. [PubMed: 22947495]

Cesare AJ, Kaul Z, Cohen SB, Napier CE, Pickett HA, Neumann AA, Reddel RR. Spontaneous occurrence of telomeric DNA damage response in the absence of chromosome fusions. Nature structural & molecular biology. 2009; 16:1244–1251.

Chapman JR, Barral P, Vannier JB, Borel V, Steger M, Tomas-Loba A, Sartori AA, Adams IR, Batista FD, Boulton SJ. RIF1 Is Essential for 53BP1-Dependent Nonhomologous End Joining and Suppression of DNA Double-Strand Break Resection. Molecular cell. 2013; 49:858–871. [PubMed: 23333305]

Chin L, Artandi SE, Shen Q, Tam A, Lee SL, Gottlieb GJ, Greider CW, DePinho RA. p53 deficiency rescues the adverse effects of telomere loss and cooperates with telomere dysfunction to accelerate carcinogenesis. Cell. 1999; 97:527–538. [PubMed: 10338216]

Crabbe L, Cesare AJ, Kasuboski JM, Fitzpatrick JA, Karlseder J. Human Telomeres Are Tethered to the Nuclear Envelope during Postmitotic Nuclear Assembly. Cell reports. 2012; 2:1521–1529. [PubMed: 23260663]

de Lange T. How shelterin solves the telomere end-protection problem. Cold Spring Harb Symp Quant Biol. 2010; 75:167–177. [PubMed: 21209389]

Deckbar D, Birraux J, Krempler A, Tchouandong L, Beucher A, Walker S, Stiff T, Jeggo P, Lobrich M. Chromosome breakage after G2 checkpoint release. The Journal of cell biology. 2007; 176:749–755. [PubMed: 17353355]

Denchi EL, de Lange T. Protection of telomeres through independent control of ATM and ATR by TRF2 and POT1. Nature. 2007; 448:1068–1071. [PubMed: 17687332]

Deng C, Zhang P, Harper JW, Elledge SJ, Leder P. Mice lacking p21CIP1/WAF1 undergo normal development, but are defective in G1 checkpoint control. Cell. 1995; 82:675–684. [PubMed: 7664346]

Dimitrova N, Chen YC, Spector DL, de Lange T. 53BP1 promotes non-homologous end joining of telomeres by increasing chromatin mobility. Nature. 2008; 456:524–528. [PubMed: 18931659]

Escribano-Diaz C, Orthwein A, Fradet-Turcotte A, Xing M, Young JT, Tkac J, Cook MA, Rosebrock AP, Munro M, Canny MD, et al. A Cell Cycle-Dependent Regulatory Circuit Composed of 53BP1-RIF1 and BRCA1-CtIP Controls DNA Repair Pathway Choice. Molecular cell. 2013; 49:872–883. [PubMed: 23333306]

Gong Y, de Lange T. A Shld1-controlled POT1a provides support for repression of ATR signaling at telomeres through RPA exclusion. Molecular cell. 2010; 40:377–387. [PubMed: 21070964]

Griffith JD, Comeau L, Rosenfield S, Stansel RM, Bianchi A, Moss H, de Lange T. Mammalian telomeres end in a large duplex loop. Cell. 1999; 97:503–514. [PubMed: 10338214]

Hayashi MT, Cesare AJ, Fitzpatrick JA, Lazzerini-Denchi E, Karlseder J. A telomere-dependent DNA damage checkpoint induced by prolonged mitotic arrest. Nature structural & molecular biology. 2012; 19:387–394.

Jackson SP, Durocher D. Regulation of DNA damage responses by ubiquitin and SUMO. Molecular cell. 2013; 49:795–807. [PubMed: 23416108]

Karlseder J, Hoke K, Mirzoeva OK, Bakkenist C, Kastan MB, Petrini JH, de Lange T. The telomeric protein TRF2 binds the ATM kinase and can inhibit the ATM-dependent DNA damage response. PLoS Biol. 2004; 2:E240. [PubMed: 15314656]

Karlseder J, Smogorzewska A, de Lange T. Senescence induced by altered telomere state, not telomere loss. Science. 2002; 295:2446–2449. [PubMed: 11923537]

Kaul Z, Cesare AJ, Huschtscha LI, Neumann AA, Reddel RR. Five dysfunctional telomeres predict onset of senescence in human cells. EMBO reports. 2012; 13:52–59. [PubMed: 22157895]

Lee HW, Blasco MA, Gottlieb GJ, Horner JW 2nd, Greider CW, DePinho RA. Essential role of mouse telomerase in highly proliferative organs. Nature. 1998; 392:569–574. [PubMed: 9560153]

Lim DS, Kim ST, Xu B, Maser RS, Lin J, Petrini JH, Kastan MB. ATM phosphorylates p95/nbs1 in an S-phase checkpoint pathway. Nature. 2000; 404:613–617. [PubMed: 10766245]

O'Sullivan RJ, Kubicek S, Schreiber SL, Karlseder J. Reduced histone biosynthesis and chromatin changes arising from a damage signal at telomeres. Nature structural & molecular biology. 2010; 17:1218–1225.

Okamoto K, Bartocci C, Ouzounov I, Diedrich JK, Yates JR 3rd, Denchi EL. A two-step mechanism for TRF2-mediated chromosome-end protection. Nature. 2013; 494:502–505. [PubMed: 23389450]

Pampalona J, Frias C, Genesca A, Tusell L. Progressive telomere dysfunction causes cytokinesis failure and leads to the accumulation of polyploid cells. PLoS genetics. 2012; 8:e1002679. [PubMed: 22570622]

Peuscher MH, Jacobs JJ. DNA-damage response and repair activities at uncapped telomeres depend on RNF8. Nature cell biology. 2011; 13:1139–1145.

Stansel RM, de Lange T, Griffith JD. T-loop assembly in vitro involves binding of TRF2 near the 3′ telomeric overhang. Embo J. 2001; 20:5532–5540. [PubMed: 11574485]

Thanasoula M, Escandell JM, Suwaki N, Tarsounas M. ATM/ATR checkpoint activation downregulates CDC25C to prevent mitotic entry with uncapped telomeres. The EMBO journal. 2012; 31:3398–3410. [PubMed: 22842784]

Waldman T, Kinzler KW, Vogelstein B. p21 is necessary for the p53-mediated G1 arrest in human cancer cells. Cancer research. 1995; 55:5187–5190. [PubMed: 7585571]

Wu J, Chen Y, Lu LY, Wu Y, Paulsen MT, Ljungman M, Ferguson DO, Yu X. Chfr and RNF8 synergistically regulate ATM activation. Nature structural & molecular biology. 2011; 18:761–768.

Highlights

- Deprotected telomeres signal differently than DNA breaks
- Deprotected telomeres do not activate the G2M checkpoint
- Intermediate-state telomeres do not activate CHK2
- Deprotected telomeres are transmitted through mitosis to arrest growth in G1 phase

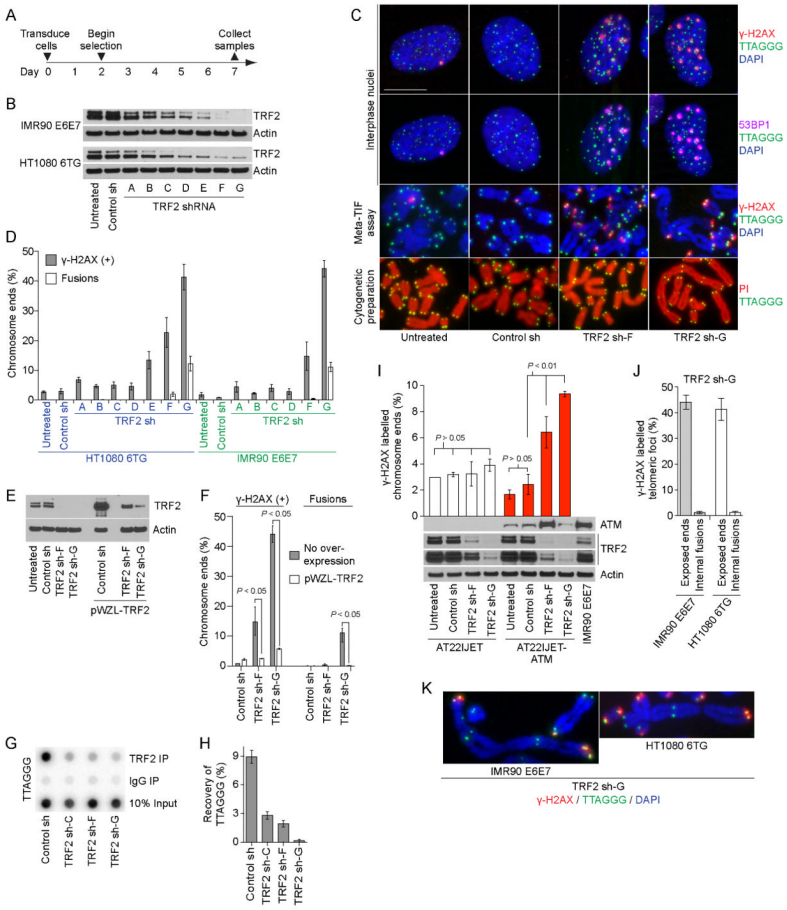

Figure 1.

Induction of intermediate- and uncapped-state telomeres. A) Timeline of the experiments in panels (B-K). B) Western blots of whole cell extracts from the indicated cultures. C) Fluorescent micrographs of IMR90 E6E7 cells. Interphase nuclei were stained with DAPI, telomere fluorescent in situ hybridization (FISH) and γ-H2AX and 53BP1 immunofluorescence (IF) and imaged in four colors. A single interphase nucleus is shown with γ-H2AX IF presented above and 53BP1 IF below. The bar is equivalent to 10 ≥m. Metaphase-TIF (Meta-TIF) assays were stained with DAPI, telomere FISH and γ-H2AX IF. Cytogenetic preparations were stained with telomere FISH and propidium iodide (PI). D) Quantitation of γ-H2AX associated telomeres in meta-TIF assays and telomere fusions in cytogenetic preparations (mean ± s.d., n = 3). E) Western blots of whole cell extracts from IMR90 E6E7 cultures with or without TRF2 overexpression (pWZL-TRF2) and shRNA transduction. F) Quantitation of meta-TIF assays and cytogenetic preparations (mean ± range, n = 2, *P* = two-tailed t-test) on the cells shown in (E). G) TRF2 ChIP of HT1080 6TG cells transduced with the indicated shRNAs. H) Quantitation of the ChIP assay shown in (G) (mean ± range, n = 2). I) Quantitation of meta-TIF assays on AT22IJET AT-cells with and without ATM complementation (mean ± s.d., n = 3, *P* = two-tailed t-test). Western blots of whole cell extracts from the indicated cell cultures are shown below. J) Comparison of γ-H2AX IF signal at exposed chromosome ends and internal fusions from meta-TIF assays of TRF2 sh-G cells (mean ± s.d., n = 3 experiments of > 130 fusions). K) Images of telomere fusions lacking γ-H2AX IF staining. See also Figure S1 and S2.

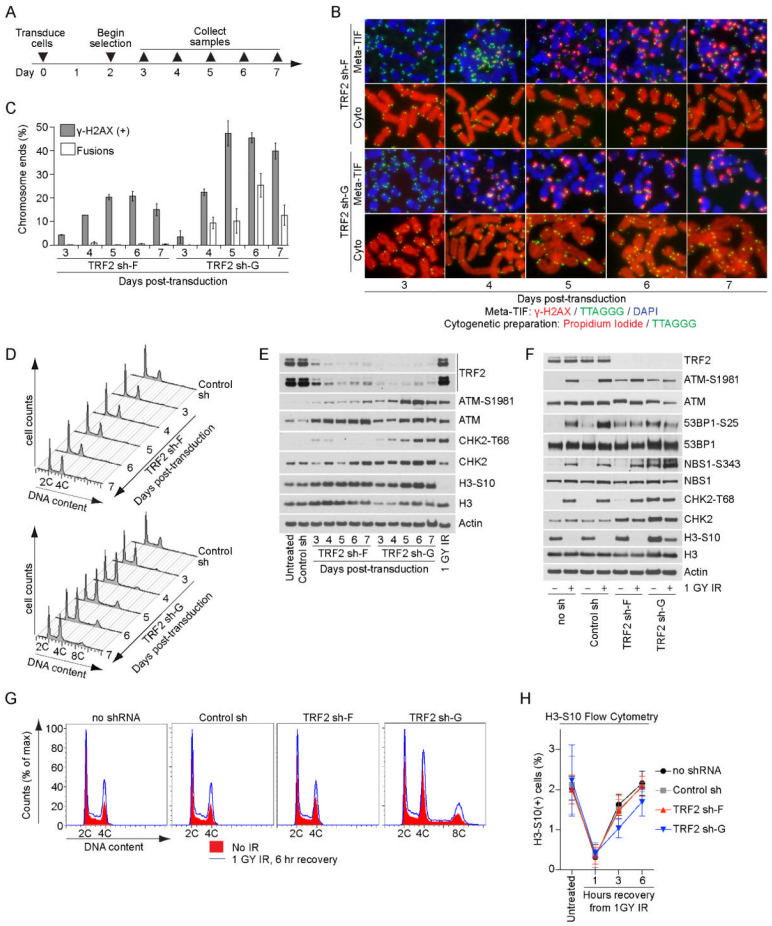

Figure 2.

TRF2 depletion does not activate the G2/M checkpoint in HT1080 6TG cells. A) Timeline of the experiments in panels (B-E). B) Examples of meta-TIF assays and cytogenetic preparations (cyto) from HT1080 6TG cells. Meta-TIF assays were stained with DAPI, γ-H2AX IF and telomere FISH and the cytogenetic preparations with PI and telomere FISH. C) Quantitation of meta-TIF assays and cytogenetic preparations (mean ± range, n = 2) depicted in (B). D) Cell cycle profiles of HT1080 6TG cultures following control or TRF2 sh transduction. A representative experiment quantifying ≥ 15,000 cells per condition is shown. E) Western blots on whole cell extracts prepared from HT1080 6TG cultures. The control shRNA sample is from seven days post-transduction and the 1GY IR sample is parental cells that recovered for one hour before sample collection. F) Western blots on whole cells extracts from untreated or irradiated HT1080 6TG cultures with or without shRNA at seven days post transduction. Irradiated cultures recovered for one hour before sample collection. G) Cell cycle profiles of untreated or irradiated HT1080 6TG cells with or without shRNA at seven days post transduction. A representative experiment quantifying ≥ 15,000 cells per condition is shown. H) Quantitation of H3-S10 positive cells in untreated or irradiated HT1080 6TG cultures with or without shRNA at seven days post transduction (mean ± s.d. n=3 experiments quantifying ≥ 25,000 cells per condition). See also Figure S3.

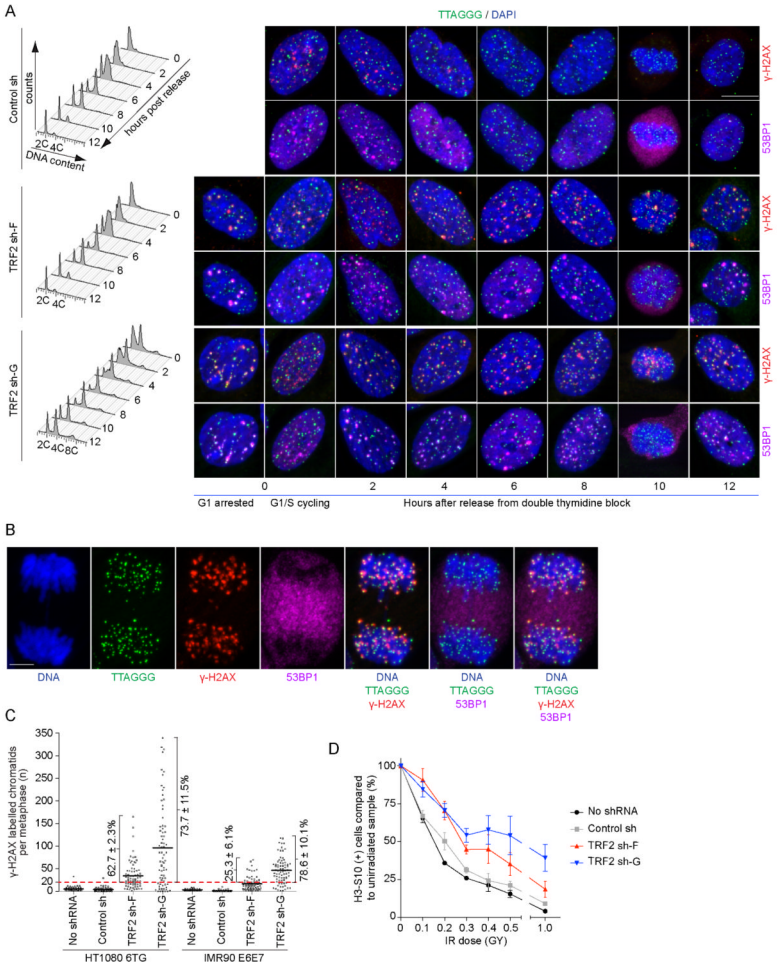

Figure 3.

Deprotected telomeres are passed on between cell cycle phases and through cell division. A) shRNA transduced IMR90 E6E7 cultures were synchronized with a double thymidine block so that at release the cultures were seven days post-transduction. Following release cells were collected every two hours for analysis by flow cytometry and fluorescent imaging. Cell cycle profiles are a representative experiment quantifying ≥ 10,000 cells per condition. Cells were stained for imaging with DAPI, telomere FISH and γ-H2AX and 53BP1 IF and imaged in four-colors. One nucleus is shown for each condition with γ-H2AX IF presented above and 53BP1 IF below. B) A representative HT1080 6TG TRF2 sh-G anaphase cell stained with DAPI, telomere FISH, γ-H2AX and 53BP1 IF. The white bar in (A) and (B) is equivalent to 10 ≥m. C) Quantitation of γ-H2AX stained telomere chromatids in meta-TIF assays on asynchronous cultures transduced with the indicated shRNAs. Individual metaphases are represented by a dot, the population average by a black bar, and the percentage of metaphases with ≥ 20 γ-H2AX(+) telomere chromatids indicated (mean ± s.d., n = 3). D) HT1080 6TG cells with or without shRNA transduction were treated with the indicated dose of IR, allowed to recover for one hour, and the number of H3-S10(+) cells determined by flow cytometry. Data are shown as the percentage of H3-S10(+) cells relative to the no IR control (mean ± s.e., n = 3 experiments of 50,000 cells per condition). See also Figure S4 and Movie S1-4.

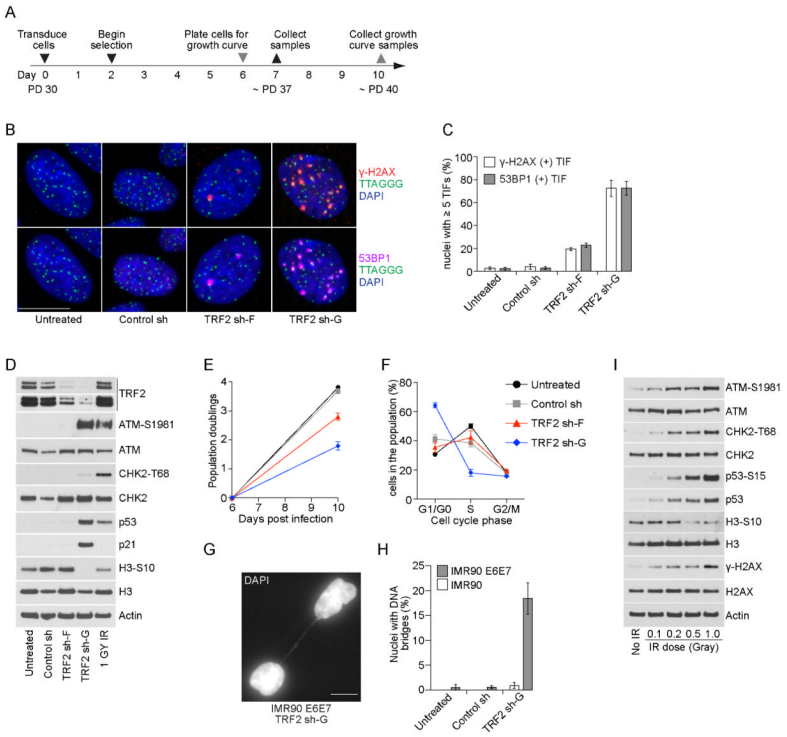

Figure 4.

Differential signaling from intermediate-state telomeres induces p53-dependent G1-phase growth arrest. A) Time line of the experiments in panels (B-H). B) Four-color imaging of IMR90 cells with our without shRNA transduction stained with DAPI, telomere FISH, γ-H2AX and 53BP1 IF. A single nucleus is shown for each condition with γ-H2AX IF above and 53BP1 IF below. C) Quantitation of interphase-TIF as shown in (B) (mean ± s.d., n = 3 experiments with typically ≥ 100 nuclei quantified). D) Western blots of whole cell extracts from untreated or shRNA transduced IMR90 cells. The 1 GY IR treated sample is parental cells that recovered for one hour before collection. E) Growth curves of untreated or shRNA transduced IMR90 cells from day six to ten post-transduction (mean ± s.d., n = 3). F) Flow cytometry determined cell cycle distribution of untreated or shRNA transduced IMR90 cells at seven days post-transduction (mean ± s.d. n = 3 experiments quantifying ≥ 10,000 cells per condition). G) Micrograph of an interphase chromatin bridge in IMR90 E6E7 TRF2 sh-G. The white bar in (B) and (G) is equivalent to 10 ≥m. H) Quantitation of inter-nuclear bridges in IMR90 and IMR90 E6E7 cultures at seven days post-transduction (mean ± s.d., n = 3 experiments quantifying ≥ 500 nuclei). I) Western blots of parental IMR90 cells treated with varying doses of IR that recovered for one hour before sample collection.

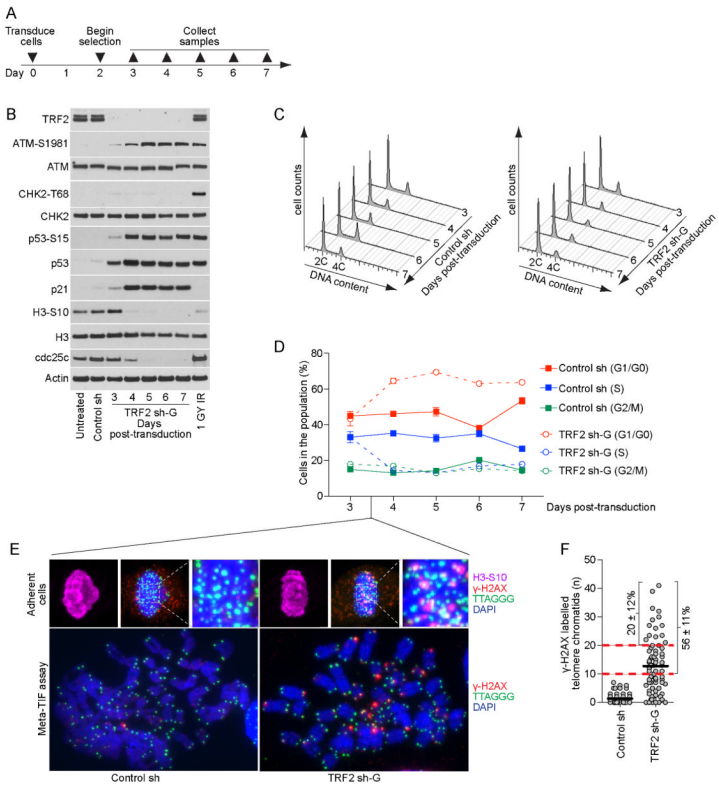

Figure 5.

Intermediate-state telomeres are passed through mitosis to arrest growth in G1-phase. A) Timeline of the experiments in panels (B-D). B) Western blots on whole cell extracts from IMR90 cultures. The control sh sample is seven days post-transduction and the 1GY IR sample are parental cells that recovered for one hour after IR before collection. C) Cell cycle profiles of control sh or TRF2 sh-G transduced IMR90 cells at days three to seven post-transduction (representative experiment quantifying ≥ 10,000 cells per condition). D) Graphical representation of the data in (C) (mean ± s.d., n = 3). E) Fluorescent micrographs of adherent mitotic cells in asynchronous culture (top) or meta-TIF assays (bottom) from control sh and TRF2 sh-G transduced IMR90 cultures at day 3.5 post-transduction. Adherent cells were stained with DAPI, telomere FISH, γ-H2AX IF and H3-S10 IF and Meta-TIF assays with DAPI, telomere FISH, and γ-H2AX IF. F) Quantitation of the meta-TIF assays shown in (E). Each metaphase is represented by a dot, the population average with a black bar and the percentage of metaphases with ≥ 10 and ≥ 20 γ-H2AX-assocaited telomere chromatids indicated (mean ± s.d., n = 3).

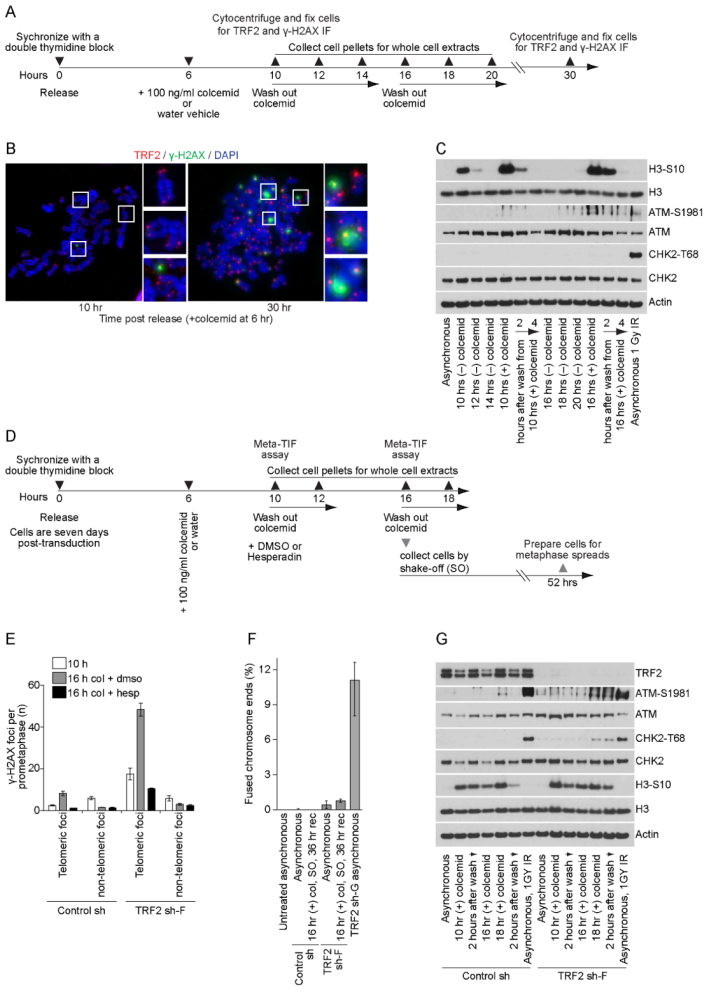

Figure 6.

The telomere-dependent prolonged mitotic arrest checkpoint signals through intermediate-state telomeres. A) Timeline of the experiments performed in IMR90 cells without shRNA transduction in panels (B, C). B) Meta-TIF assays performed on IMR90 cultures treated as shown in (A). Samples were stained with DAPI, γ-H2AX IF and TRF2 IF. C) Western blots on whole cell extracts from IMR90 cultures treated as shown in (A). D) Timeline of the experiments on control sh or TRF2 sh-F transduced IMR90 E6E7 cells shown in panels (E-G). Cells were seven days post-transduction when released from the double thymidine block. E) Quantitation of meta-TIF assay experiments in IMR90 E6E7 control shRNA and TRF2 sh-F cells as shown in Figure S5 (mean ± s.d. n = 3). Cells were treated as shown in (D) and Figure S5. F) Quantitation of fused chromosome ends in cytogenetic preparations following 36 hours of recovery after shake-off isolation of IMR90 E6E7 Control shRNA or TRF2 sh-F cells undergoing a prolonged mitotic arrest (mean ± range, n ≥ 2). Cells were treated as shown in (D) without Hesperadin or DMSO treatment 10 hrs post-release. G) Western blots of whole cell extracts prepared from IMR90 E6E7 Control shRNA or TRF2 sh-F cells following prolonged mitotic arrest. Cells were treated as shown in (D) without Hesperadin or DMSO treatment 10 hrs post-release. Irradiated cultures recovered for one hour before sample collection. See also Figure S5.

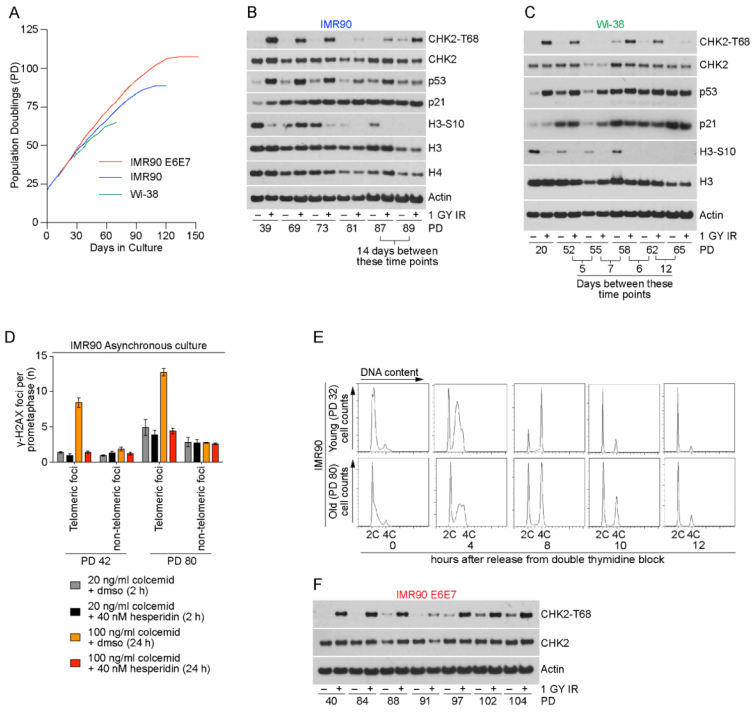

Figure 7.

Spontaneous DDR signaling is consistent with intermediate-state telomeres at senescence and uncapped-state telomeres at crisis. A) Growth curves of IMR90, IMR90 E6E7 and WI-38 fibroblasts in hypoxic conditions used in panels (B-F). B and C) Western blots of whole cell extracts from IMR90 or WI-38 cultures with or without irradiation at the indicated population doublings. Irradiated cultures recovered for one hour before sample collection. D) Quantitation of meta-TIF experiments shown in Figure S6. Asynchronous young or aged IMR90 cells were treated with 40 nM Hesperadin or DMSO and either 20 ng/ml colcemid for two hours or 100 ng/ml colcemid for 24 hours before sample preparation (mean ± s.d. n = 3). E) Cell cycle profiles of young or aged IMR90 cultures following synchronization with a double thymidine block and release (a representative experiment of ≥ 15,000 cells per condition is shown). F) Western blots of whole cell extracts from IMR90 E6E7 cultures with or without irradiation at the indicated population doublings. Irradiated cultures recovered for one hour before sample collection. See also Figure S6.